Singlet Oxygen Generation as a Major Cause for Parasitic Reactions during Cycling of Aprotic Lithium-Oxygen Batteries

Nika Mahne[1], Bettina Schafzahl[1], Christian Leypold[1], Mario Leypold[3], Sandra Grumm[1], Anita Leitgeb[1], Gernot A. Strohmeier[3,4], Martin Wilkening[1], Olivier Fontaine[5,6], Denis Kramer[7], Christian Slugovc[1], Sergey M. Borisov[2] and Stefan A. Freunberger[1]*

[1] Institute for Chemistry and Technology of Materials, Graz University of Technology, Stremayrgasse 9, 8010 Graz, Austria

[2] Institute for Analytical Chemistry and Food Chemistry, Graz University of Technology, Stremayrgasse 9, 8010 Graz, Austria

[3] Institute of Organic Chemistry, Graz University of Technology, Stremayrgasse 9, 8010 Graz, Austria

[4] acib - Austrian Centre of Industrial Biotechnology GmbH, Petersgasse 14, 8010 Graz, Austria

[5] Institut Charles Gerhardt Montpellier, UMR 5253, CC 1701, Université Montpellier, Place Eugène Bataillon, 34095 Montpellier Cedex 5, France

[6] Réseau sur le Stockage Electrochimique de l'Énergie (RS2E), FR CNRS

[7] Engineering Sciences, University of Southampton, SO17 1BJ, Southampton, UK

* to whom correspondence should be addressed: freunberger@tugraz.at

Supplementary Figures

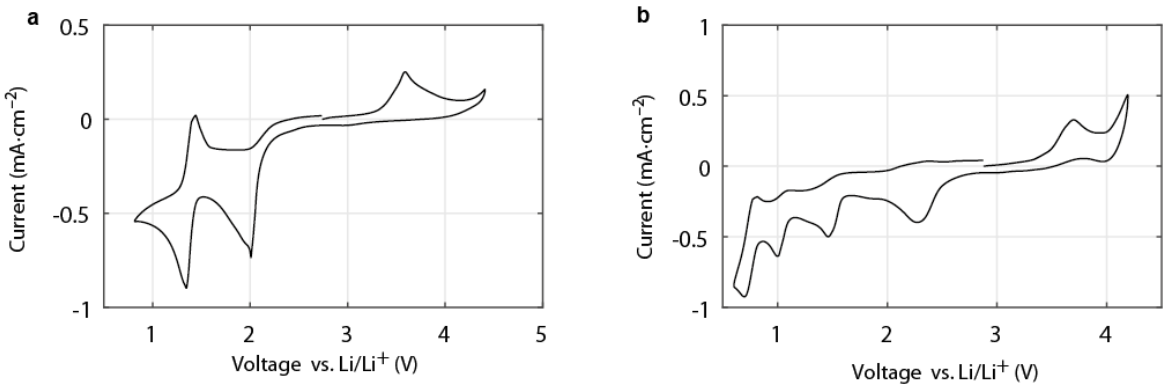

Supplementary Figure 1 | Electrochemistry of typical chromophores used in fluorescent $^1O_2$ probes. **a**, fluorescein, **b**, rhodamine 6G.

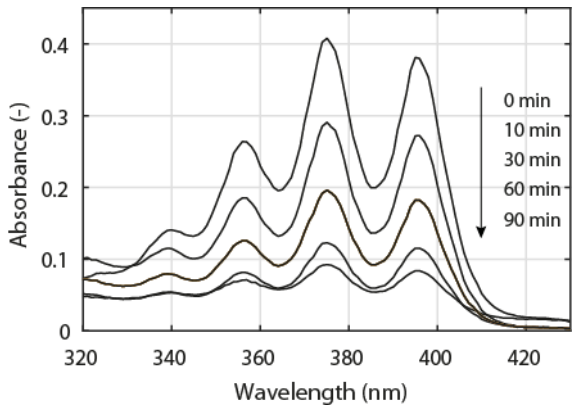

Supplementary Figure 2 | Reaction of 9,10-diphenylanthracene with singlet oxygen to 9,10-diphenylanthracene-endoperoxide. UV-Vis absorption spectra of a 3.0×10^{-5} M solution of 9,10-diphenylanthracene, in TEGDME containing palladium(II) *meso*-tetra(4-fluorophenyl)tetrabenzoporphyrin upon illumination for the times indicated. The absorbance is dimensionless, thus there is no unit.

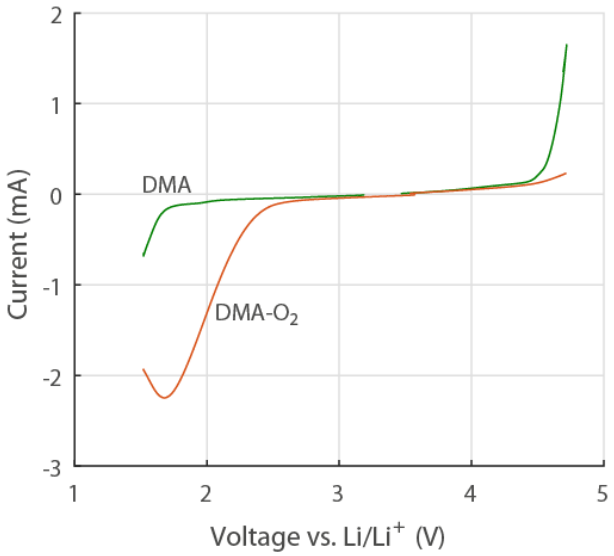

Supplementary Figure 3 | Electrochemical stability of 9,10-dimethylanthracene (DMA) and 9,10-dimethylanthracene-endoperoxide (DMA-O_2). Cyclic voltammetry was performed at a 3 mm glassy carbon disc electrode at a sweep rate of 100 $mV \cdot s^{-1}$. First 2 mM DMA and 0.1 M $LiClO_4$ in TEGDME were measured under Ar-atmosphere, $^1O_2$ was then generated photochemically with the sensitizer palladium(II) *meso*-tetra(4-fluorophenyl)tetrabenzoporphyrin under O_2-atmosphere and then the formed DMA-O_2 was measured under Ar-atmosphere.

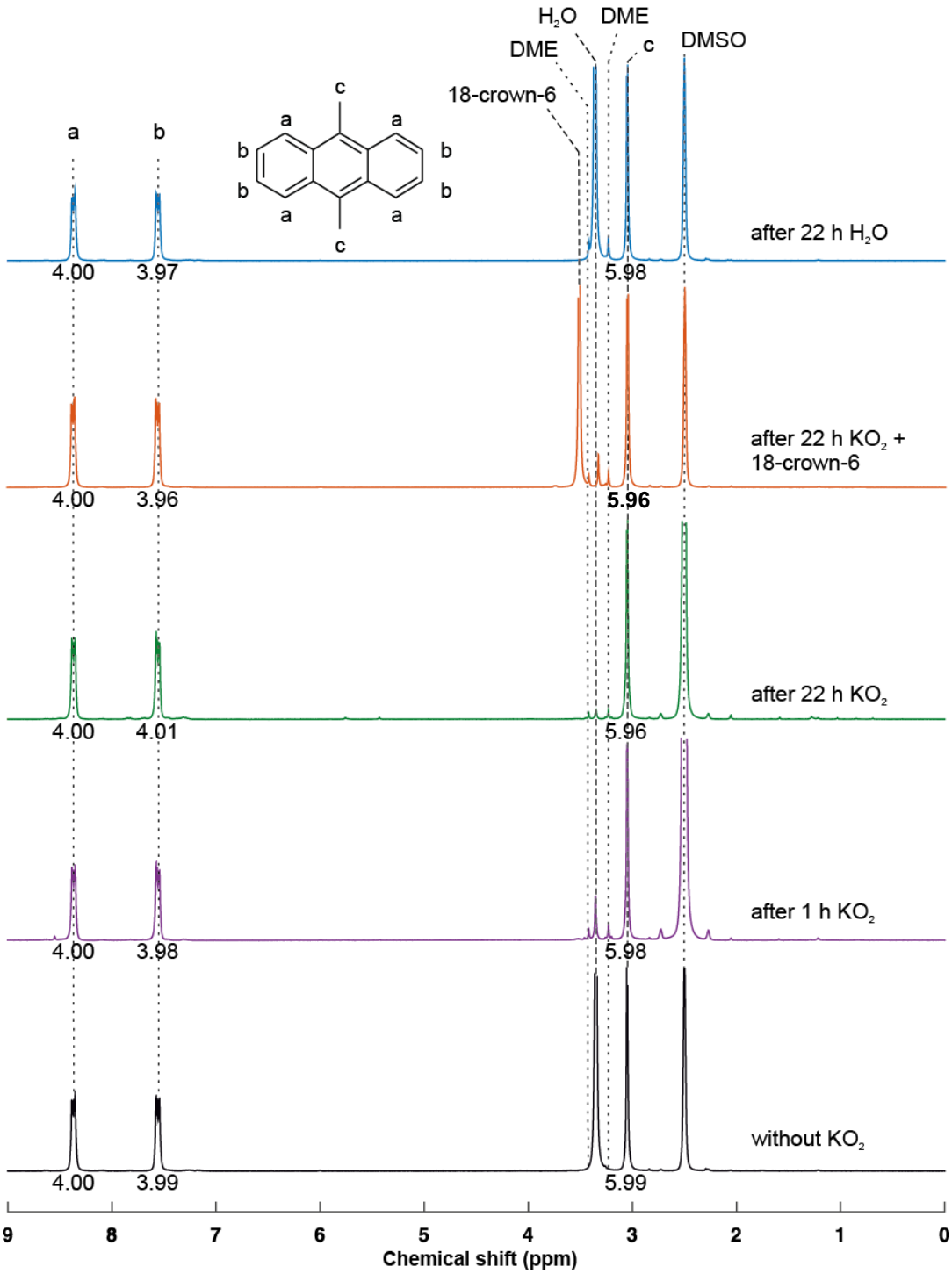

Supplementary Figure 4 |Stability of DMA in contact with KO_2 or H_2O in 0.1 M $LiClO_4$ in DME. A solution of 4×10^{-2} M DMA in dry DME containing 0.1 M $LiClO_4$ was stirred with an excess of KO_2 and ^{1}H-NMR samples taken after the times indicated. For the orange curve the solution contained additionally an excess of 18-crown-6. The electrolyte solvent was evaporated and the remainder dissolved in d_6-DMSO. Analogously for the top-most spectrum 1000 ppm H_2O were added to a solution of 4×10^{-2} M DMA in DME containing 0.1 M $LiClO_4$ and a ^{1}H-NMR sample taken after the time indicated. The letters a, b, c denote the peaks of the DMA and the numbers underneath the integrals, where the integrals for the proton a is normalized to 4. Peaks associated with DME, DMA, 8-crown-6, H_2O, and DMSO are indicated. The small peaks symmetric to the DMSO peak are satellites.

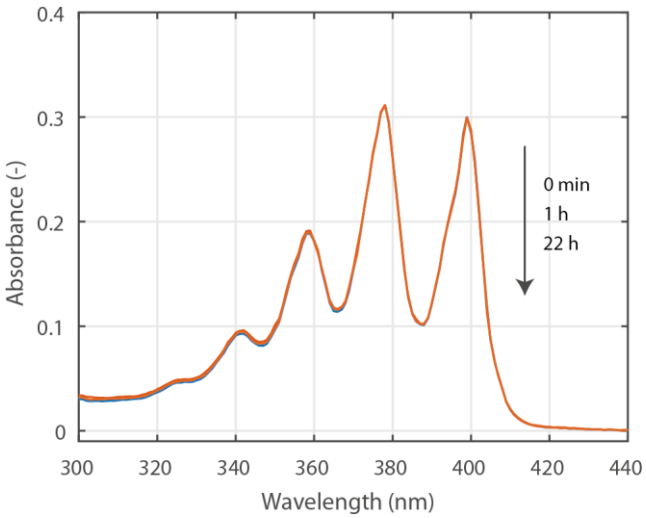

Supplementary Figure 5 | UV-Vis absorption spectra of 9,10-dimethylanthracene in contact with KO_2 in DME. A solution of 2.5×10^{-5} M DMA in DME was stirred with an excess of KO_2. UV-Vis absorption spectra were recorded at the times indicated. The absorbance is dimensionless, thus there is no unit.

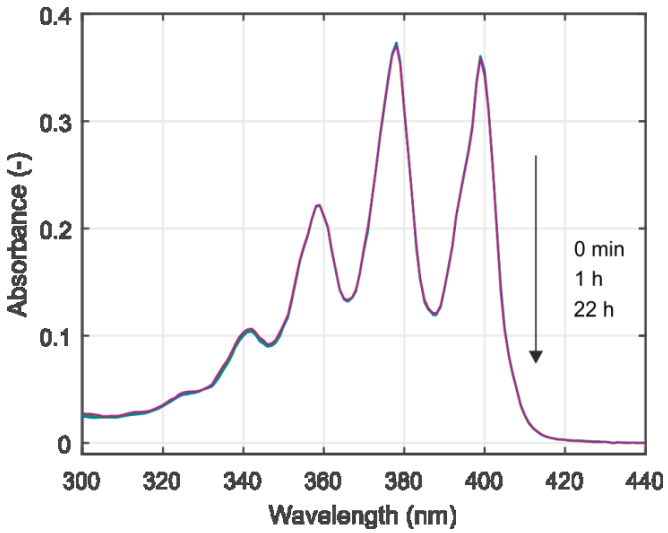

Supplementary Figure 6 | Stability of 9,10-dimethylanthracene in presence of 1000 ppm H_2O in 0.1 M $LiClO_4$ in DME. A solution of 3.0×10^{-5} M DMA in DME was stirred in presence of 1000 ppm H_2O. UV-Vis absorption spectra were recorded at the times indicated. The absorbance is dimensionless, thus there is no unit.

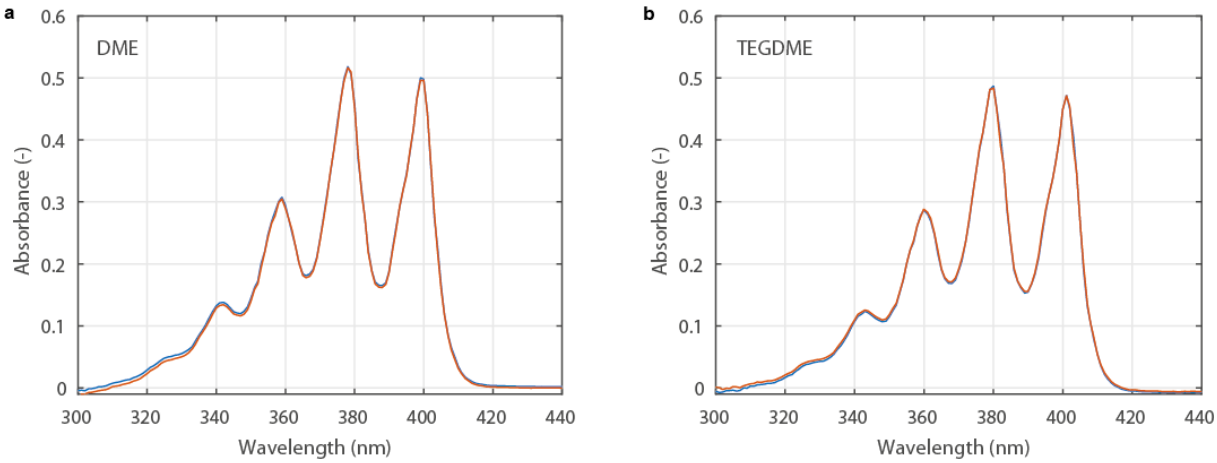

Supplementary Figure 7 | Stability of DMA in contact with KO_2 in DME and TEGDME containing 18-crown-6. A solution of 4×10^{-2} M DMA in dry DME or TEGDME containing 0.1 M $LiClO_4$ was mixed with both an excess of KO_2 and the crown ether 18-crown-6 and UV-Vis samples were taken before KO_2 addition and after 22h. The samples were diluted 1/600 in the respective solvent to yield a measurable absorbance. The absorbance dimensionless, thus there is no unit.

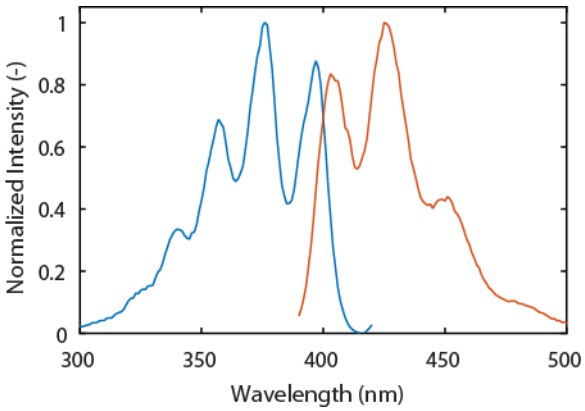

Supplementary Figure 8 | Excitation and emission spectra of 9,10-dimethylanthracene in 0.1 M $LiClO_4$ in TEGDME. The excitation (blue trace) was recorded from 280nm – 420nm with λ_{em}= 425nm. The emission (orange trace) was recorded from 380nm-700nm with λ_{ex}= 378nm.

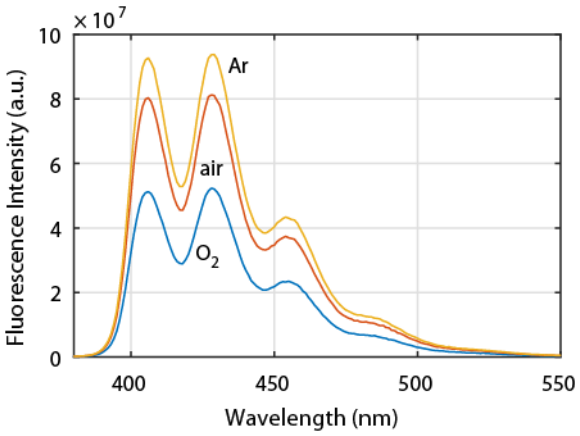

Supplementary Figure 9 | Quenching of DMA fluorescence by varying O_2 concentrations. Emission spectrum of 1.6×10^{-5} M DMA in 0.1 M $LiClO_4$ in TEGDME that is either purged with Ar, dry air or pure O_2. The excitation wavelength was λ_{ex} = 378 nm.

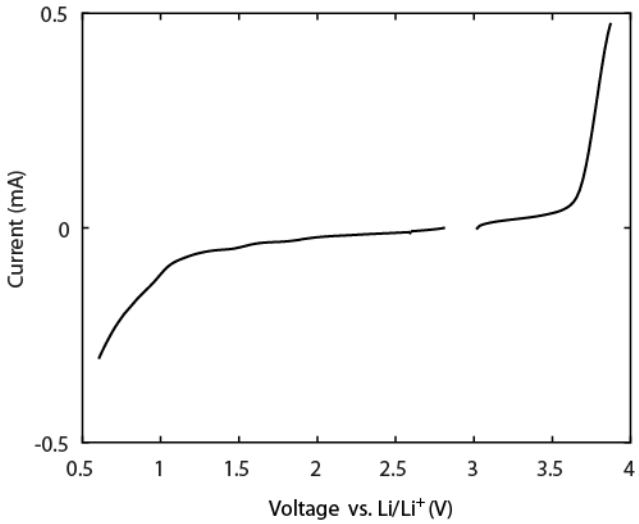

Supplementary Figure 10 | Electrochemical stability of DABCO. Cyclic voltammogram of 2 mM DABCO and 100 mM $LiClO_4$ in TEGDME at an Au-disc electrode with a scan rate of 100 $mV\cdot s^{-1}$.

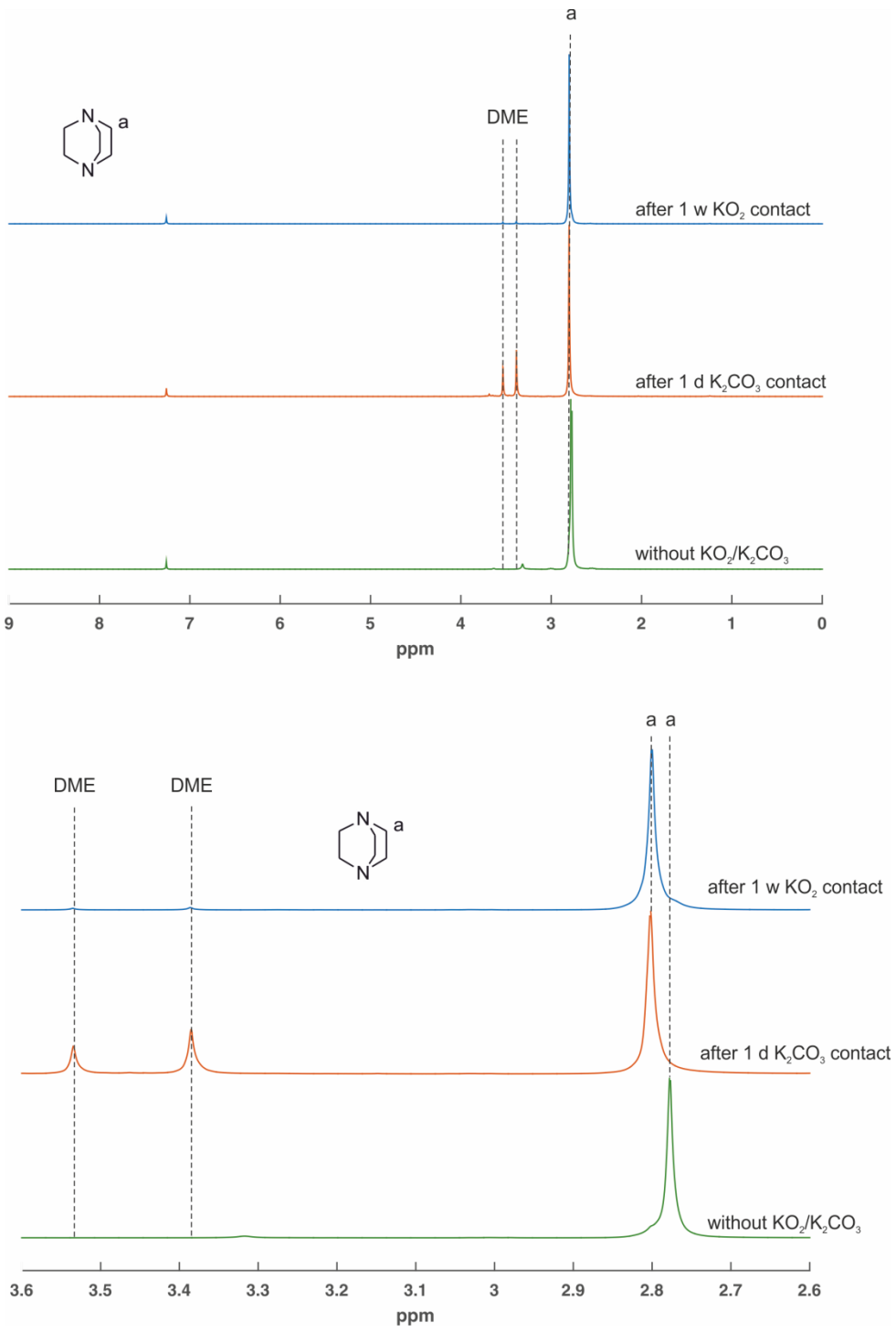

Supplementary Figure 11 | Stability of DABCO in contact with KO_2 in 0.1 M $LiClO_4$ in DME. A solution of 9×10^{-2} M DABCO in DME containing 0.1 M $LiClO_4$ was stirred with an excess of KO_2 and ^{1}H-NMR samples taken after the times indicated. The electrolyte solvent was evaporated and the remainder dissolved in $CDCl_3$. The peak at 7.26 ppm is the $CHCl_3$ peak.

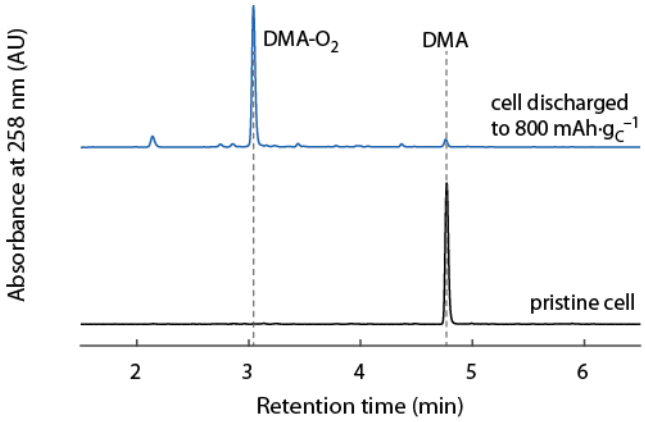

Supplementary Figure 12 | HPLC-MS analysis of DMA containing electrolyte after operation in an Li-O_2 cell for the quantification of DMA and DMA-O_2. A typical HPLC chromatogram of the electrolyte extracted from a Li-O_2 cell after galvanostatic cycling. The MS signal was used to identify the retention times for DMA and DMA-O_2 which were found to be 4.7 min and 3.1 min. The DMA signal showed up in the mass spectrum at $[M+H]^+$ 207 m/z (calcd 207.1 m/z), whereas the DMA-O_2 signal showed up at $[M+H]^+$ 239 m/z (calcd 239.1 m/z).

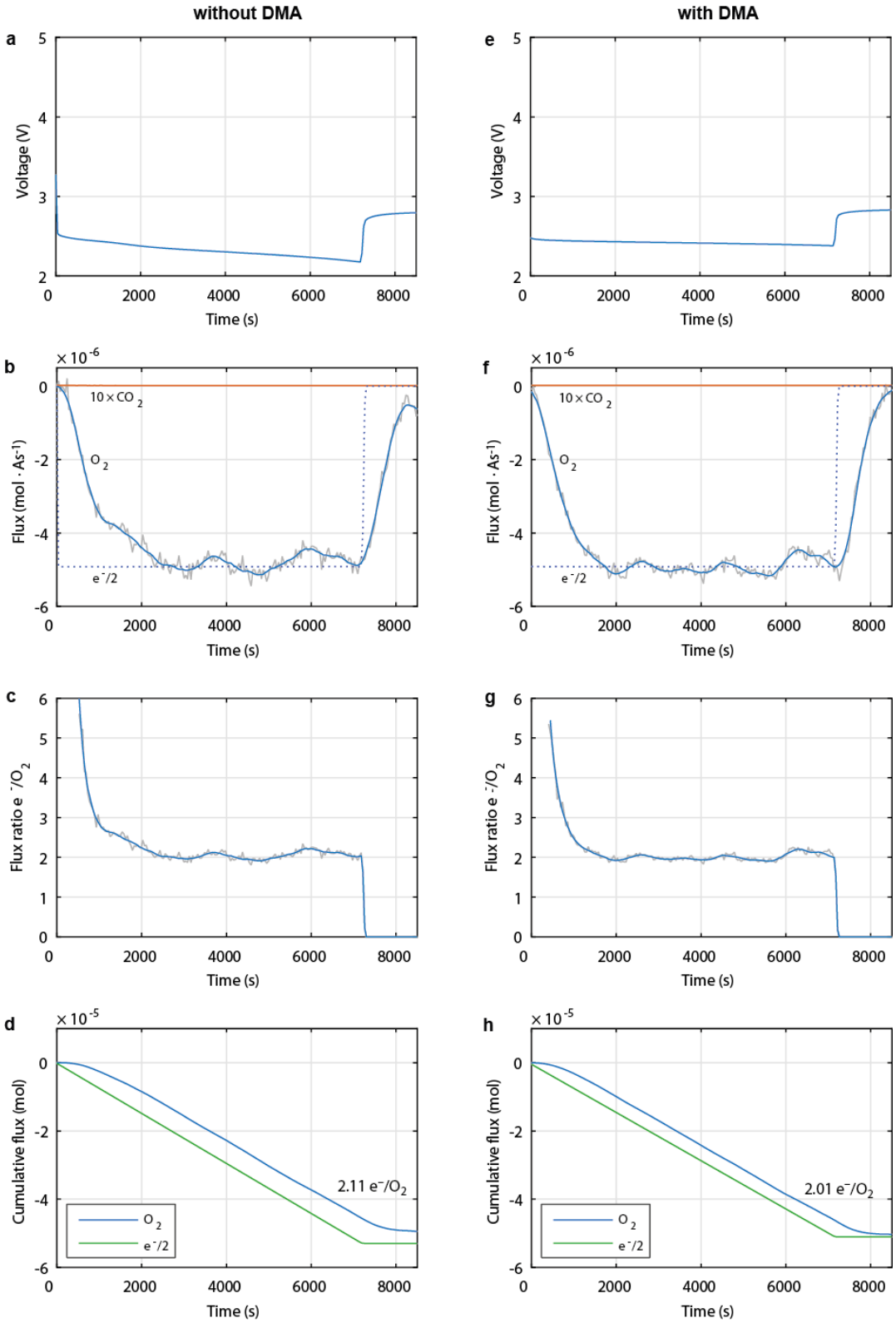

Supplementary Figure 13| *Operando* electrochemical mass spectrometry during discharge of Li-O_2 cathodes to 200 mAh·g_C^{-1} with electrolytes containing either no additive or DMA. a to **d**, without DMA. Voltage profiles (**a**), fluxes of O_2, e^-, and CO_2 (**b**), e^-/ O_2 ratio (**c**), cumulative fluxes of O_2 and e^- (**d**). **e** to **h**, with DMA. Voltage profiles (**a**), fluxes of O_2, e^-, and CO_2 (**b**), e^-/ O_2 ratio (**c**), cumulative fluxes of O_2 and e^- (**d**). Cells were run at 70 mA·g_C^{-1} in 0.1 M $LiClO_4$ in TEGDME containing either no additive or 30 mM DMA.

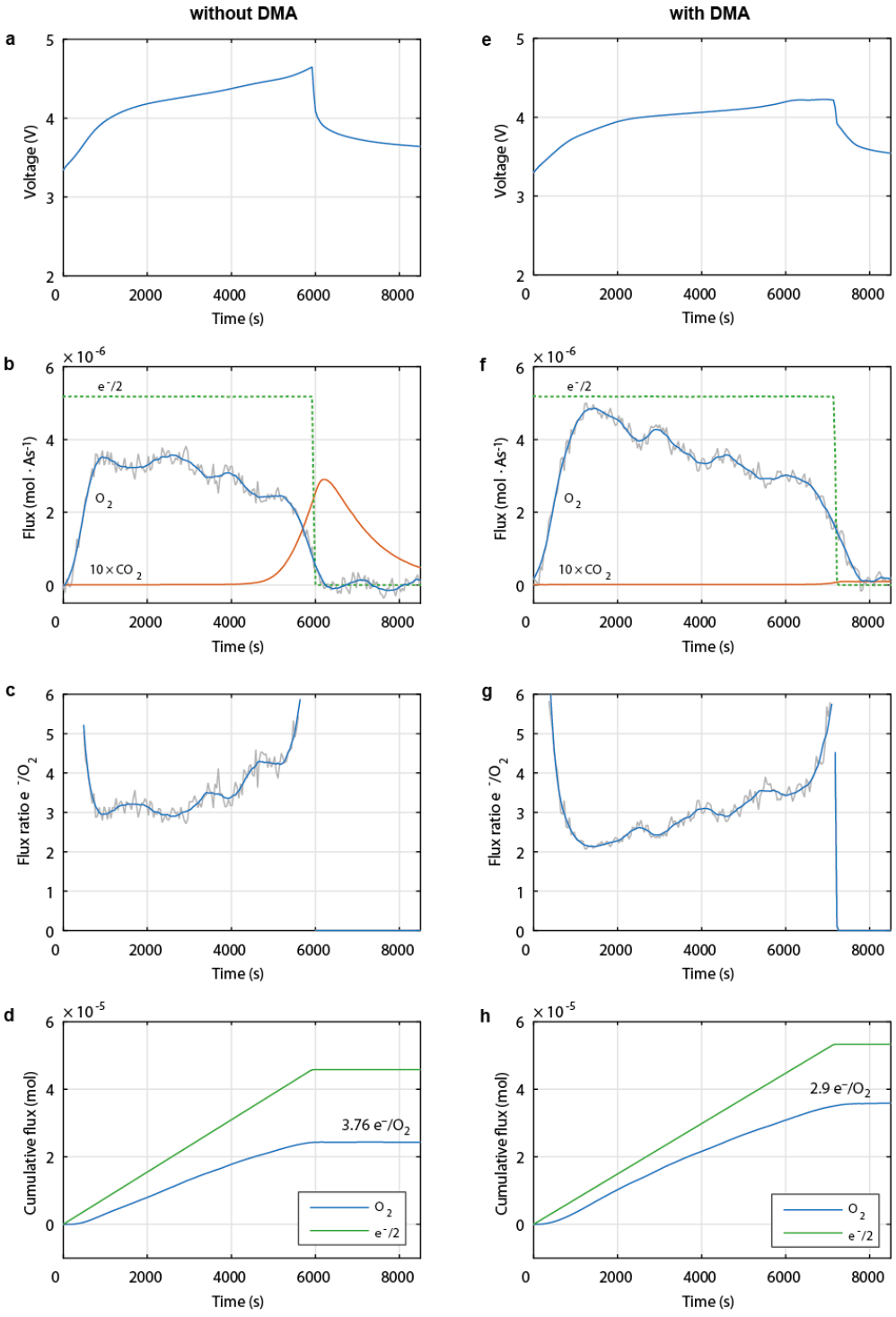

Supplementary Figure 14| *Operando* electrochemical mass spectrometry during charge of Li-O_2 cathodes after discharge to 200 mAh·g_C^{-1} with electrolytes containing either no additive or DMA. a to **d**, without DMA. Voltage profiles (**a**), fluxes of O_2, e^-, and CO_2 (**b**), e^-/ O_2 ratio (**c**), cumulative fluxes of O_2 and e^- (**d**). **e** to **h**, with DMA. Voltage profiles (**a**), fluxes of e^-, and CO_2 (**b**), O_2, e^-/ O_2 ratio (**c**), cumulative fluxes of O_2 and e^- (**d**). Cells were run at 70 mA·g_C^{-1} in 0.1 M $LiClO_4$ in TEGDME containing either no additive or 30 mM DMA.

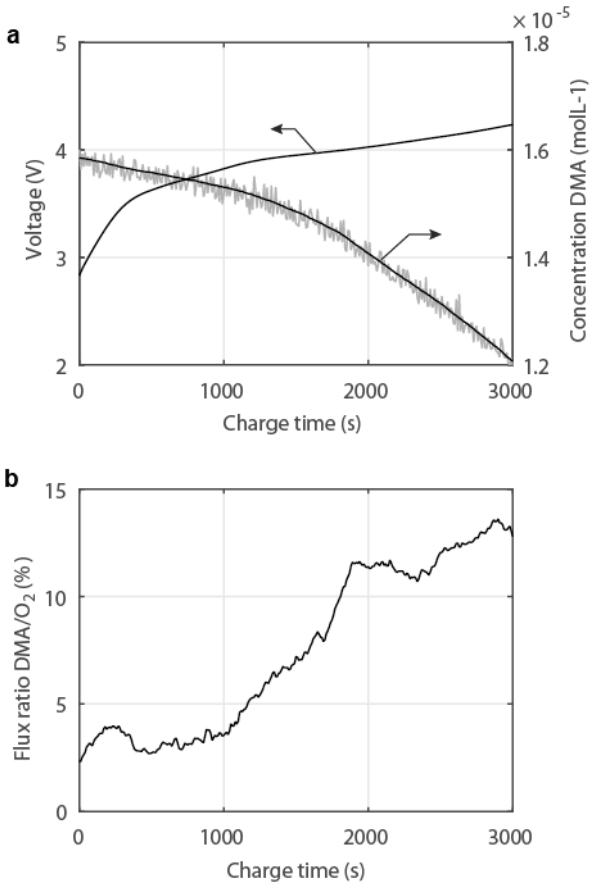

Supplementary Figure 15 | DMA consumption rate in relation to the theoretical O_2 evolution rate as derived from Fig. 2b. a, Voltage profile and DMA concentration as a function of charge time. **a**, Ratio of DMA consumption rate ($\mathrm{d}n_{\mathrm{DMA}}/\mathrm{d}t$) and theoretical O_2 evolution rate ($\mathrm{d}n_{\mathrm{O2}}/\mathrm{d}t$, based on current).

Supplementary Table

Supplementary Table 1 | Amount of side products as a function of discharge capacity as shown in Fig. 4b.

	No additive	DMA		DABCO	
Discharge capacity ($mAh \cdot g_C^{-1}$)	mol CO_2/mg_C $\times 10^{-6}$	mol CO_2/mg_C $\times 10^{-6}$	Fraction vs. no additive	mol CO_2/mg_C $\times 10^{-6}$	Fraction vs. no additive
400	2.00	0.86	43 %	0.67	34 %
800	2.60	0.79	32 %	0.36	14 %
1200	3.43	2.81	82 %	1.13	33 %
			37 ± 6 % average[1)]		**27 ± 10 % average**

[1)] For averaging the sample at 1200 $mAh \cdot g_C^{-1}$ with DMA was ignored since no DMA was present any more from the second sample point onwards, see Fig. 4c.

Supplementary Discussion

Fraction of parasitic reactions due to singlet oxygen

Supplementary Figure S11 investigates the stability of DABCO versus superoxide. DABCO was dissolved in 0.1 M $LiClO_4$ and was stirred with an excess of KO_2 and ^{1}H-NMR samples taken after the times indicated. Even after one week there is no change in the spectra visible. Note that the nitrogen coordinates to the cation and shifts the CH_2 peak in comparison to DABCO alone in the NMR solvent. That the shift after KO_2 addition originates from this is demonstrated by analogously bringing DABCO in contact with K_2CO_3, which affords the same shift as seen in the red trace.

Estimating the fraction of parasitic reactions due to $^1O_2$ is easier on discharge and the value can be estimated from Fig. 4b. As mentioned in the text neither DMA nor DABCO will necessarily divert all formed $^1O_2$ from building side products. Therefore the observed amount of side reaction products is not the same for DMA and DABCO and can be considered as still partially stemming from $^1O_2$. The values are summarized in Supplementary Table 1. DABCO appears to be the more effective agent. In average DMA reduces the amount of side products to ~37%, DABCO to ~27%. From the value with DABCO we deduce that some ~70 % of the side products are related to $^1O_2$ on discharge. This supports our interpretation that the majority of parasitic products on discharge is due to $^1O_2$.

Estimating the fraction of the parasitic products due to $^1O_2$ on charge is more difficult than on discharge. This is because of two reasons: First, the discharge product will not be 100% Li_2O_2 and oxidation current therefore not 100% related to Li_2O_2 oxidation. Second, DMA will gradually be consumed on charge and at a much higher rate than on discharge as seen in Fig. 2. Nevertheless, conditions at the start of charge, when most of the DMA is still present will give a good indication.

The O_2 evolution rate missing to the theoretical rate can be considered an approximate measure for the rate at which $^1O_2$ is formed and diverted into building parasitic products. In the case shown in Fig. 5 without DMA (orange curve) roughly one third of the theoretical O_2 evolution rate is missing at the start of charge and more than half missing towards the end of charge. As mentioned a significant part of the current will not be related to Li_2O_2 oxidation and an estimation of the fraction of the parasitic products due to $^1O_2$ on charge will be unreliable.

For the case with DMA (green curve) the discharge product can be regarded as much purer Li_2O_2 than without DMA and the O_2 evolution rate reaches ~93% of the theoretical value. This value can be understood when considering the rate at which DMA is consumed on charge during the operando fluorescence measurement in Fig. 2b. It must be kept in mind that in the fluorescence experiments the DMA concentration was only 16 µM which is why the DMA consumption rate will present a lower boundary of the $^1O_2$ formation rate. Supplementary Fig. 15 shows the DMA consumption rate in relation to the theoretical O_2 evolution rate (based on current) as derived from Fig. 2b. DMA is consumed (as $^1O_2$ is formed) at a rate of ~4-5% of the O_2 evolution rate at the onset of charge, which is in reasonable agreement with the ~93% O_2 evolution rate in online MS, Fig. 5. Therefore the under-evolution of O_2 can be interpreted as being linked to $^1O_2$ generation. Further support for this interpretation comes from the comparison of CO_2 evolution with and without DMA, Fig. 5b. The dramatic decrease of CO_2 with DMA suggests that the species responsible for parasitic products on charge ($^1O_2$) has overwhelmingly been eliminated by the DMA (the $^1O_2$ trap). Taken together, these results suggest that the majority of the parasitic products that form during charge are due to the occurrence of $^1O_2$.

Proton assisted singlet oxygen formation

A more in depth discussion of possible $^1O_2$ formation mechanisms is given in the following. When H_2O or other proton sources is available the superoxide will be protonated to form HOO• (Eq. 2) that has been reported to either undergo reduction by superoxide (Eq. 3) or disproportionate (Eq. 4) [1-3] and to be able to release in either case $^1O_2$ [4-7].

$$O_2^- + H^+ \rightarrow HOO\bullet \quad (2)$$

$$HOO\bullet + O_2^- \rightarrow HO_4^- \rightarrow HOO^- + {}^1O_2 \quad (3)$$

$$2\,HOO\bullet + H_2O \rightarrow H_2O_4 \rightarrow H_2O_2 + H_2O + {}^1O_2 \quad (4)$$

With the overall reaction

$$2\,O_2^- + 2\,H^+ \rightarrow H_2O_2 + {}^1O_2 \quad (5)$$

H_2O_2 is believed to further react with HOO^- to form the highly reactive hydroxyl radical

$$H_2O_2 + HOO^- \rightarrow H_2O + HO\bullet + O_2^- \quad (7)$$

whereas the reaction $H_2O_2 + O_2^- \rightarrow OH^- + HO\bullet + {}^1O_2$ was shown to be unfavourable[8].

Supplementary References

1 Andrieux, C. P., Hapiot, P. & Saveant, J. M. Mechanism of superoxide ion disproportionation in aprotic solvents. *J. Am. Chem. Soc.* **109**, 3768-3775, (1987).

2 Chin, D. H., Chiericato, G., Nanni, E. J. & Sawyer, D. T. Proton-induced disproportionation of superoxide ion in aprotic media. *J. Am. Chem. Soc.* **104**, 1296-1299, (1982).

3 Che, Y. *et al.* Water-induced disproportionation of superoxide ion in aprotic solvents. *J. Phys. Chem.* **100**, 20134-20137, (1996).

4 Corey, E. J., Mehrotra, M. M. & Khan, A. U. Water induced dismutation of superoxide anion generates singlet molecular oxygen. *Biochemical and Biophysical Research Communications* **145**, 842-846, (1987).

5 Khan, A. U. Direct spectral evidence of the generation of singlet molecular oxygen (1.Delta.G) in the reaction of potassium superoxide with water. *J. Am. Chem. Soc.* **103**, 6516-6517, (1981).

6 Koppenol, W. H. Reactions involving singlet oxygen and the superoxide anion. *Nature* **262**, 420-421, (1976).

7 Mayeda, E. A. & Bard, A. J. Singlet oxygen. Suppresion of its production in dismutation of superoxide ion by superoxide dismutase. *J. Am. Chem. Soc.* **96**, 4023-4024, (1974).

8 Stanley, J. P. Reactions of superoxide with peroxides. *J. Org. Chem.* **45**, 1413-1418, (1980).